Surface Science 278 (1992) 146–156
North-Holland

surface science

A scanning tunneling microscopy and spectroscopy study of the $TiO_{2-x}(110)$ surface

Gregory S. Rohrer
Department of Materials Science and Engineering, Carnegie Mellon University, Pittsburgh, PA 15213, USA

Victor E. Henrich
Surface Science Laboratory, Department of Applied Physics, Yale University, New Haven, CT 06520, USA

and

Dawn A. Bonnell
Department of Materials Science and Engineering, University of Pennsylvania, Philadelphia, PA 19104, USA

Received 21 February 1992; accepted for publication 4 July 1992

The surface structure of reduced $TiO_{2-x}(110)$ has been studied in ultrahigh-vacuum by scanning tunneling microscopy and tunneling spectroscopy. A variety of surface structure types with periodicities larger than the bulk TiO_2 unit cell have been clearly resolved. These periodic structures, which have repeat distances ranging from 3.2 Å to greater than 30 Å, coexist with one another on the reduced surface and have domain sizes of < 1000 Å. Tunneling spectra acquired from this surface show the bulk conduction band edge 0.5 eV above the Fermi level and a bandgap greater than 2.5 eV. These observations are compared to a surface structure model that assumes the presence of varying concentrations of bulk crystallographic shear plane defects that accommodate non-stoichiometry in this material.

1. Introduction

Transition metal oxide surfaces are known to mediate a number of interesting processes including the reactions that underlie some catalytic phenomena. TiO_2 is one of the most thoroughly studied oxides, and previous investigations of its surface structure using traditional ultrahigh vacuum (UHV) surface probes have yielded a great deal of information on the average structure of the perfect and defective surfaces [1–5]. However, the development of atomistic models to explain surface processes also requires a detailed knowledge of the real-space surface structure, including the geometry, population, and electronic characteristics of surface defects. In an attempt to acquire such information, we have carried out scanning tunneling microscopy (STM) and tunneling spectroscopy (TS) experiments on the reduced $TiO_2(110)$ surface which are described in this paper.

The rutile structure consists of chains of edge-sharing TiO_6 octahedra, aligned along the c-axis, which link at vertices to form the three-dimensional structure shown in fig. 1. Titania has a wide range of possible oxygen stoichiometry (TiO_{2-x}, where $0.33 \geq x \geq 0$) that is accommodated in the near stoichiometric region by the formation of oxygen vacancies and for larger x by the formation of planar defects known as crystallographic shear (CS) planes, along which normally corner-sharing octahedra transform to an

edge-sharing arrangement [6]. As the concentration of CS planes increases, the defects order to form distinct structures that have the general formula Ti_nO_{2n-1}. Each of these structures, known as Magnéli phases, can be thought of as consisting of small volumes of the uncorrupted rutile structure that are joined together along the CS planes. The formation of substoichiometric TiO_2 is signaled by the transformation of the stoichiometric, colorless, transparent crystal to a blue, n-type semiconductor. The donors that give rise to the n-type conductivity for small deviations from stoichiometry are thought to be O vacancies or Ti interstitials, while in the Magnéli phases further off stoichiometry the donors are believed to be the reduced Ti cation pairs that reside along the CS planes [7].

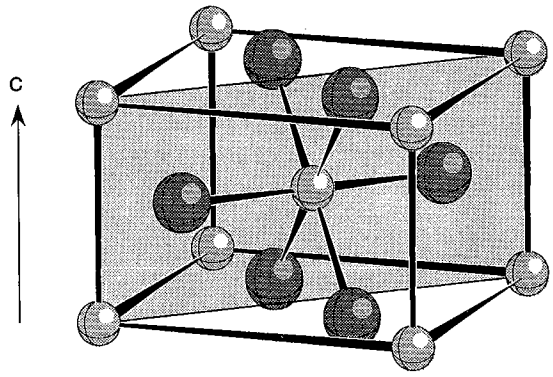

(A)

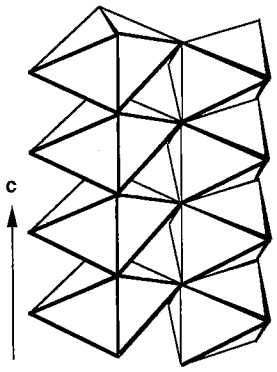

(B)

Fig. 1. (A) The rutile unit cell. Ti atoms are represented by the smaller spheres with lighter shading. (B) The three-dimensional structure is formed by columns of edge sharing octahedra which link at vertices.

The (110) surface of an idealized rutile crystal that is produced by breaking the fewest number of bonds is shown in fig. 2A. The rows of oxygen atoms oriented in the [001] direction are called "bridging oxygens", while the ones in the plane below are referred to as "in-plane". Both this structure and the one shown in fig. 2B, in which the bridging oxygens have been eliminated, are consistent with (1×1) low energy electron diffraction (LEED) patterns observed on vacuum fractured surfaces. Vacuum annealed surfaces sometimes exhibit (2×1) LEED patterns, but the origin of this symmetry is unknown [1]. Small degrees of oxygen deficiency in the surface region (TiO_{2-x} with $x < 10^{-4}$) might be accommodated by isolated oxygen vacancies, which could occur in either bridging or in-plane positions. Larger deviations from stoichiometry could be accommodated by the formation of CS planes in the near-surface region. Both missing oxygen atoms and the shear displacements associated with the CS planes would result in geometric alterations in the titania surface structure.

Ultraviolet photoelectron spectroscopy (UPS) experiments indicate that the electronic structure of the TiO_2(110) surface is essentially the same as that of the bulk. This conclusion is supported by the theoretical work of Munnix and Schmeits [8], which indicates that the orbitals associated with cations and anions on perfect TiO_2 surfaces occur as resonances that overlap the valence and conduction bands instead of states within the bulk bandgap. A mid-gap electronic state within the bulk bandgap has, however, been detected on vacuum-annealed and ion-bombarded surfaces [1]. This state lies approximately 1.0 eV below the conduction band edge and is related to surface reduction. The state is believed to be the result of the partial occupation of the Ti 3d levels of the metal cations adjacent either to oxygen vacancies [1] or to face-sharing octahedra at CS planes [5].

Numerous papers have appeared that describe STM analysis of TiO_2 surfaces [9–16]. Most of the studies have been carried out in air or liquid, conditions under which the ultimate resolution is

limited by surface contamination and charging effects. Nonetheless, some atomic-scale features have been observed. Sakamaki et al. [12] report observing an individual phenol molecule on the TiO_2(100) surface, and Fan and Bard [15] observed a square lattice structure on the (100) surface. In contrast to that work, the experiments described here were carried out under UHV conditions, which allows atomically clean surfaces to be prepared.

2. Experimental

A $1.0 \times 5 \times 1.6$ mm^3 titania sample was oriented to within $\pm 1/2°$ of the (110) face by Laue diffraction. The surface was polished by sequentially reducing the size of Al_2O_3 grinding media down to 1 μm. The crystal was then reduced in UHV by annealing in a resistively heated tantalum boat at a temperature above 900 K (based upon color) for 36 h. Following this treatment,

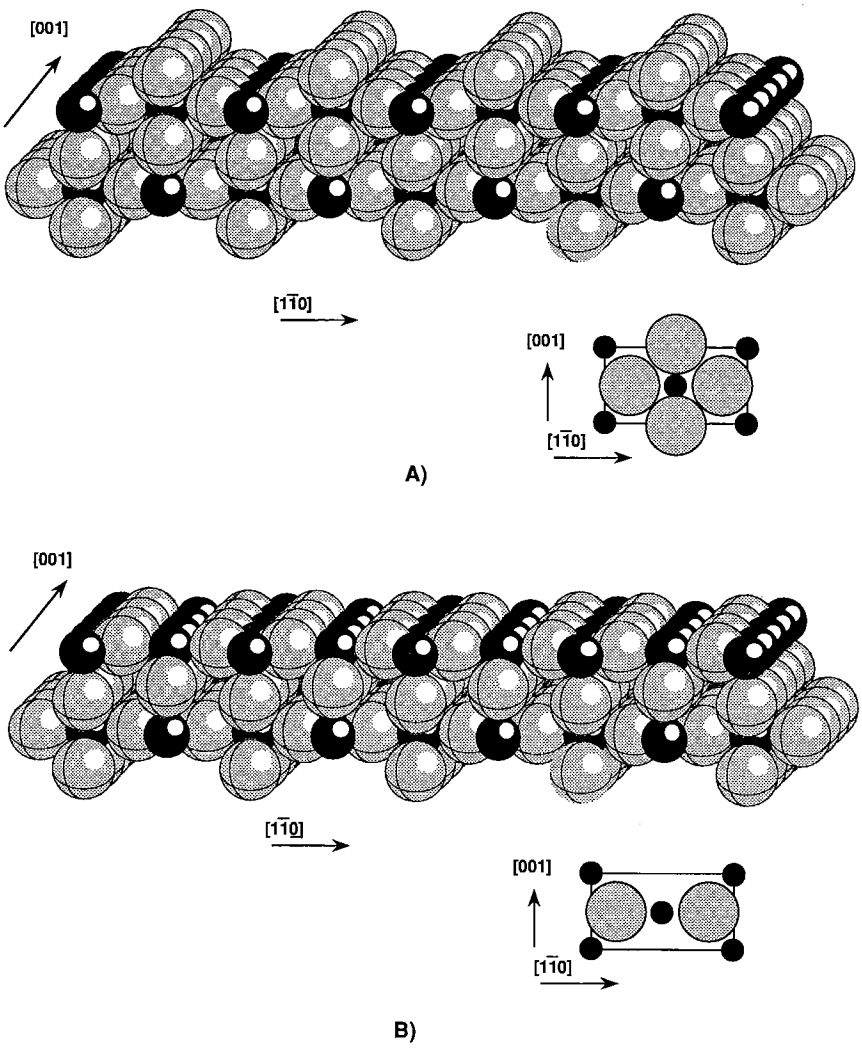

Fig. 2. Two views of the rutile (110) surface. (A) This model includes the bridging oxygen atoms that complete the coordination polyhedron of one-half of the surface titanium atoms. The surface unit viewed normal to the surface is also shown. (B) The same model, without the bridging oxygens.

the crystal was dark gray in color and opaque. The surface was then argon-ion milled for 5 min at 2 keV followed by 25 min of ion bombardment at 500 eV using an estimated current density of 5 to 10 $\mu A/cm^2$. The crystal was then annealed at 823 K for 30 min in 1×10^{-7} Torr of oxygen in order to re-oxidize the surface and anneal out the damage produced by ion bombardment. Low energy electron diffraction (LEED) patterns indicated a well-ordered, relatively defect-free surface [17]. The crystal was then exposed to air for several days before being introduced into the UHV STM chamber. In UHV it was heated to approximately 673 K for 2 min and then "flashed" to approximately 973 K for 5 s. A (1×1) LEED pattern was found after this treatment that was identical to that observed following the initial preparation. All of the data presented here were taken within 48 h of such a thermal treatment. Orientation of the crystal during STM analysis was determined from the LEED pattern. The orientation of the images is within $\pm 10°$ of the crystal orientation, the primary source of error being thermal drift.

We imaged the sample using a commercial STM head [18] controlled by feedback electronics and software of conventional design. A clipped Pt tip was "sharpened" in situ by applying a 90 V potential between the sample and tip and passing 1 μA of current for several minutes. The procedure had to be repeated periodically to maintain tip resolution and stability. In each case, the tip was repositioned following the sharpening to guard against the possibility of imaging deposited Pt. The dependence of the tunneling current on sample–tip separation was used to gauge the integrity of the vacuum gap. The standard vacuum tunneling equation was used to compute values of the effective barrier height [19], which was found to be between 4.2 and 5.0 eV for this sample. All of the images we present here were collected in the constant current mode at a +2.0 V sample bias with respect to the tip and a 0.1 nA tunneling current and are a representative selection of more than 30 images recorded over a period of several days on a single specimen. The images are presented after the subtraction of a background plane, which eliminates the tilt that would otherwise overwhelm small variations and make atomic features undetectable. Image tilts have a number of sources and the most difficult to estimate is the vertical thermal drift which varies with fluctuations in the room temperature and the rate at which the images are acquired. Images presented here had tilts ranging from 4° to 10°. The current–voltage (IV) characteristics of the tunnel junction were periodically measured during image acquisition using a method described elsewhere [20].

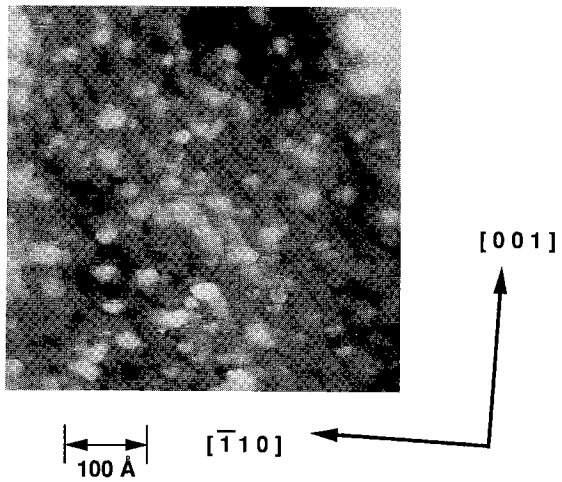

Fig. 3. STM image of a 492×492 Å^2 of the TiO_2(110) surface showing the first structure type. The vertical displacement from black to white is 5 Å.

3. Results

Several types of ordered regions were detected on the titania surface which we classify into three categories or structure types. The primary characteristic of the first structure type is meandering steps, approximately 1.0 Å in height with an average separation of 33 Å. Actual widths vary by several ångströms, and an example of this structure is shown in fig. 3. Throughout the image small "dots" protrude from the surface which in the upper half are arranged along diagonal lines, and in the bottom half are arranged in a triangular pattern. The repetition of these two motifs

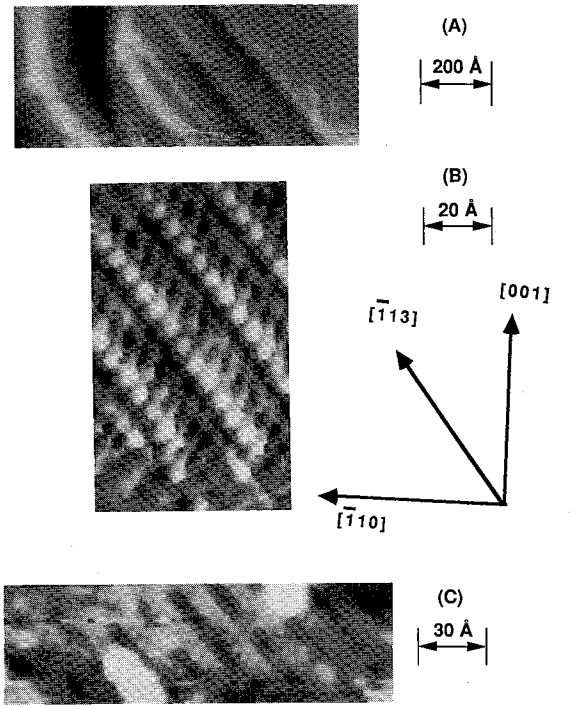

Fig. 4. STM images of the second structure type. (A) An image of a 957×383 Å^2 area of the TiO_2 surface. The vertical displacement from black to white is about 45 Å. (B) Image (63×100 Å) obtained from a higher resolution scan of one of the terraces shown in (A). (C) Enlarged subset (194×60 Å^2) of the image in (A) showing a different topographic pattern.

leads us to believe that the structures are related to tip asperities rather than the topography of the sample surface.

The second structure type is characterized by the roughly 21 Å rows oriented in the [$\bar{1}$13] direction that can be seen in fig. 4. Fig. 4A shows a large terraced region, while figs. 4B and 4C, extracted from subsequent high resolution scans of different terraces, show the two characteristic surface topographies found in this region. The rows in fig. 4B consist of 21 Å long "links" separated by approximately 6 Å which in turn appear to be made up of three sub-units, approximately 6 Å in diameter. The corrugation height of these units is 0.7 Å. Of these three sub-units, the one at the lower left edge appears larger than the other two. In rows observed on an adjacent terrace (fig. 4C), there are only two white sub-units of comparable size that make up each link, together with an "empty" position which appears black.

The third structure type, an example of which is shown in fig. 5, is characterized by rows oriented along the [1$\bar{1}$1] direction. The row width was determined from several images either by direct measurement or with a 2D Fourier transform. The period of the corrugation varied from 8 to 9 Å, depending on the image and the measurement method. The corrugation height, which was approximately 1 Å, also varied from image to image, presumably because of changes in tip shape. An additional corrugation with an amplitude as large as 0.2 Å and a wavelength of approximately 3.2 Å is apparent within each row. This elliptical shape, roughly 3 × 9 Å^2, defines a

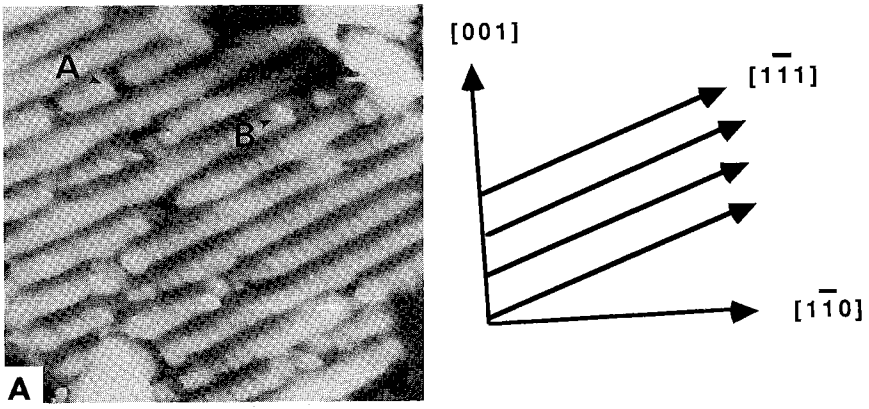

Fig. 5. STM image of 109 × 109 Å^2 area showing the third structure type.

basic unit of the surface structure that should contain roughly 5–10 atoms, based upon the ideal TiO_2 structure. Two types of defects can be observed that are commensurate with this surface unit, the first of which is labeled A on fig. 5. This hole, or missing cell, 0.7 Å deep. The second type is what appears to be an extra cell, labeled B, and appears as a protrusion or white spot on the top view image with a height that equals the depth of the hole. Another type of disorder apparent on the surface consisted of large amorphous protrusions, examples of which appear in the upper and lower parts of the image.

Two other areas that exhibited rows oriented in ⟨111⟩ directions, similar to the structure discussed above, are shown in fig. 6. These images are included to demonstrate that, while the rows often appear ordered and regular, as in figs. 4 and 5, the row structure does not always fall into one of the three categories discussed above. For example, the rows in fig. 6B are 12 Å wide while the rows in fig. 6A vary in periodicity from 6.3 to 12 Å. The configuration of the rows in this area of the surface was observed reproducibly and is not the result of random changes in the tip. Portions of each surface are covered by protrusions that appear as white regions on the image. It appears that one of these protrusions, in the upper left quadrant of the image, moved under the influence of the tip since it abruptly disappears while other image features are continuous across this line. We assume that these features are contaminants, most likely carbon, which adsorb from the background gases in the chamber. This conclusion is based on the observation that the surface carbon concentration (measured by Auger electron spectroscopy (AES)) increased during the 48 h exposure to the background gases in the chamber between thermal treatments. It is interesting to note the the contaminants sometimes have an orientational relationship to the underlying lattice. For example, in fig. 6A the features are elliptical in shape and have their major axis oriented along the direction of the rows.

Frequent and unpredictable changes in tip resolution make it difficult to estimate exactly what portion of the ordered surface was occupied by

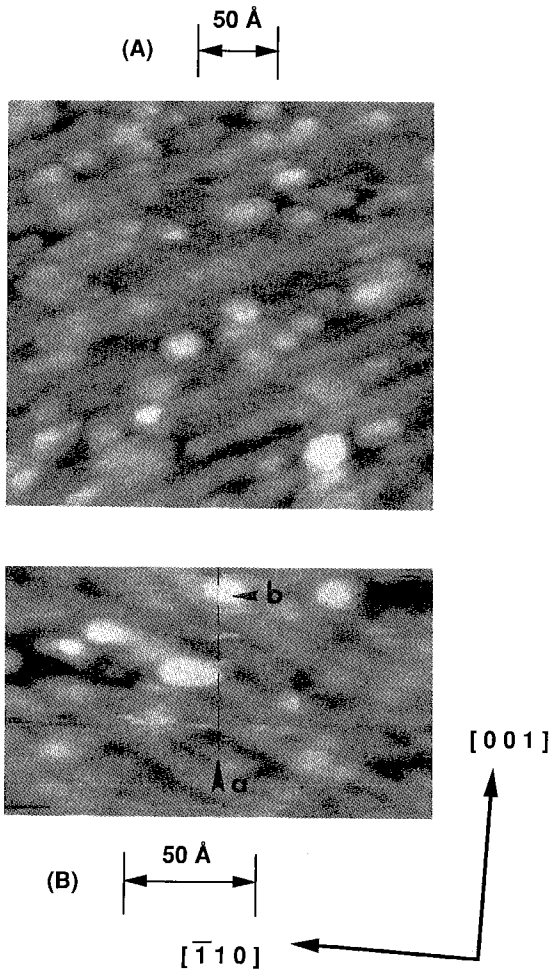

Fig. 6. Images showing a recognizable periodicity, yet with characteristic surface disorder. (A) 273×273 Å^2 image with rows oriented in the [1$\bar{1}$1] direction and (B) 164×109 Å^2 image with rows oriented in the [$\bar{1}$11] direction.

each of these structure types or even what portion of the surface was ordered. However, when tip conditions were stable, about half of the surface appeared to be ordered (that is to say, possessing a regular or semi-regular row structure such as those presented above), and images of flat regions that were 500 to 1000 Å in each dimension usually showed more than one of the ordered regions, suggesting that the typical domain size is less than 1000 Å.

Tunneling spectroscopic data were acquired during the acquisition of the image presented in

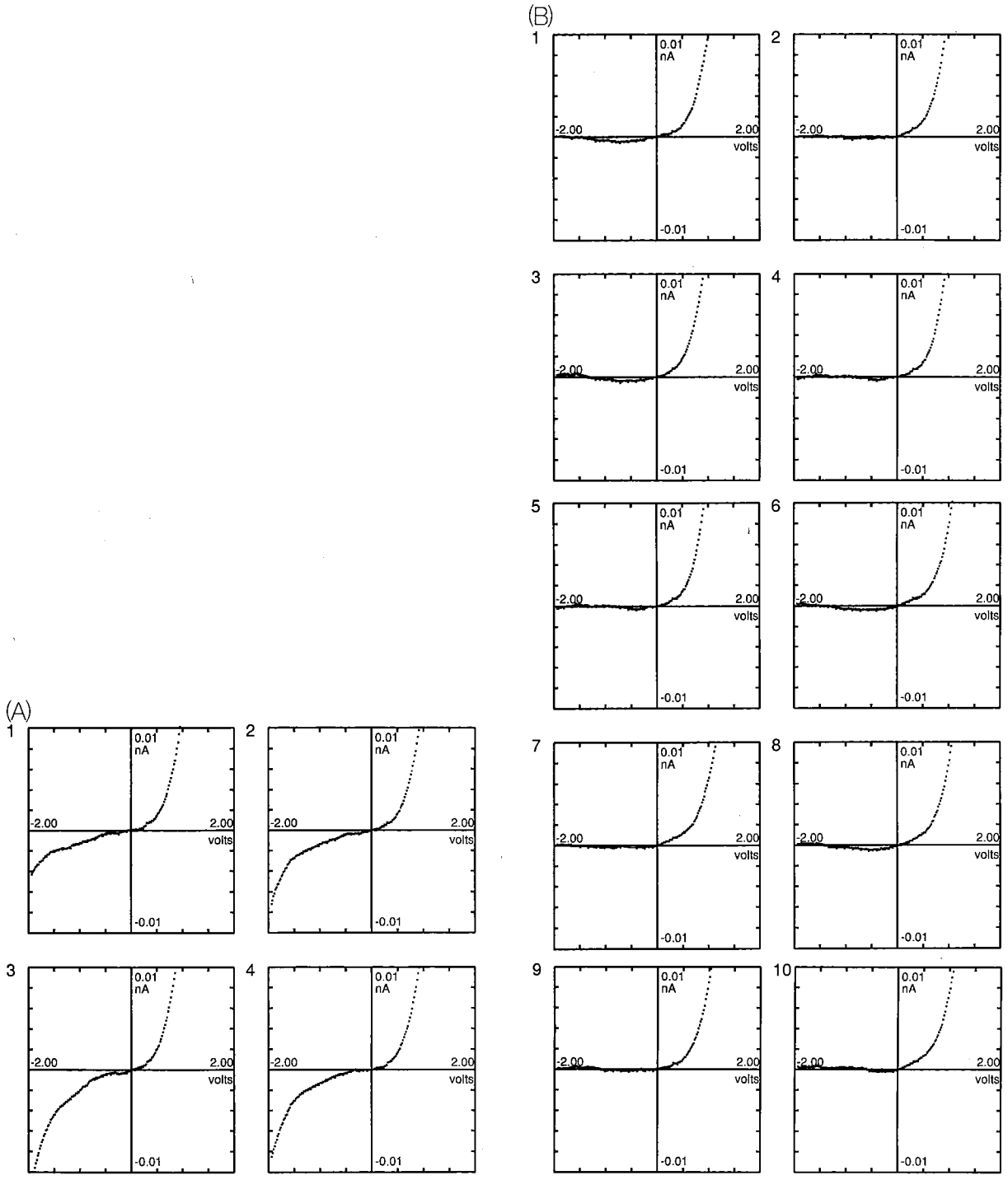

Fig. 7. *IV* curves obtained during the acquisition of the image in fig. 6B. (A) A sequence of 4 *IV* curves acquired at 1.6 Å intervals as the tip passed from top to bottom over the white protrusion labeled "b" in fig. 6B. (B) A sequence of 10 *IV* curves acquired at 1.6 Å intervals as the tip passed from top to bottom over the area of the bare surface labeled by the arrow in fig. 6B.

fig. 6B. Although the rows with 12 Å periodicity are easily discerned, detail within the rows is absent, suggesting that the resolution was limited by the tip geometry. More than 60 *IV* curves were recorded at 1.6 Å intervals along the vertical line labeled "a" in fig. 6B. These curves fall into two representative categories, those acquired as the tip passed over one of the white protrusions (this occurs twice) and those acquired from the bare surface. Fig. 7A shows a series of 4 *IV* curves sequentially recorded at 1.6 Å intervals as the tip passed from top to bottom over the center of the white feature labeled "b" in fig. 6B. Data recorded as the tip passed near the edge of the second feature are similar. Fig. 7B shows a series of 10 *IV* curves sequentially recorded at 1.6 Å intervals as the tip passed from top to bottom over the section of bare surface labeled by the arrow. The curves are labeled 1 through 10, as the tip moved from the point to the base of the arrow. These spectra are representative of those acquired from other areas of the bare surface.

There are several features of note in these curves. On the bare surface no significant current is detected at negative biases. On the other hand, as the tip passed over the protrusions, negative current is detected. Also, in the positive bias regions of the *IV* curves, the data from both regions are similar. The current rises immediately as the Fermi level (0 bias) is crossed, first at a reduced slope (0 to 0.5 eV), and then at a steeper slope (0.5 to 2.0 eV). Finally, although the data from the bare surface sequentially samples a length of 16 Å, significant variations from point to point are not observed.

4. Discussion

The STM images presented here indicate that a variety of structure types occur on the TiO_{2-x}(110) surface when reduced in UHV. A bulk termination of the rutile unit cell to form a (110) surface would produce a rectangular surface unit cell with dimensions 2.96 Å in the [001] direction and 6.50 Å in the [1$\bar{1}$0] direction. The obvious absence of correlation between this model and the observed structures indicates that the situation is more complex. One possible explanation is that the surface structure is affected by surface or subsurface deviations in stoichiometry. Assuming that this is the case, two possibilities might arise. The first is that the observed surface patterns are the result of an ordered arrangement of oxygen vacancies, and the second is that intergrowths of Magnéli phases form in the near-surface regions and that the shear displacements give rise to the observed surface corrugations. Each of these possibilities are considered in turn.

The geometries of the experimentally observed surface structures can be created by removing oxygen from the surface layer in the appropriate pattern; we call this the ordered-surface oxygen vacancy model. However, we believe that the observed corrugations of 1 Å could not result from this model for the following reason. An STM image is not simply a reproduction of the surface geometry, but also depends on the surface density of states, and both effects must be considered together. Because all of the images were acquired at positive sample bias, electrons tunneled into *unoccupied* conduction band states, which are predominantly Ti in origin. In order for a 1 Å corrugation to appear in the constant current STM image, the unoccupied states on the Ti atom must extend 1 Å more or less into the vacuum either through a geometric displacement of the atom or a change in atomic volume upon reduction. While both of these occur as the result of the O vacancy formation, neither can be as large as 1 Å. We should also consider the simple fact that O removal will, to some extent, increase the availability of Ti states at the O site and thus cause a topographic rise. However, two other effects are expected to act in opposition. The first is that two electrons are left behind at each vacancy with the removal of an O atom, and those electrons partially occupy normally empty Ti states on the neighboring cations, thus making them inaccessible at positive sample bias. The second is that any increase in available unoccupied Ti state density associated with exposure of a larger number of Ti atoms to the tip would be partially compensated by the topographic depression caused by the vacancy. Considering these opposing effects on the surface topography, it

does not seem likely that oxygen vacancies would be capable of producing surface corrugations as large as 1 Å.

The second model, the crystallographic shear (CS) model, provides a more reasonable explanation for the observed results. The assumption at the heart of this model is that the major row corrugations are actually steps that would result naturally from CS displacements. The CS displacements can occur along a variety of planes including the {121} family of planes. The (121) plane intersects the (110) surface along the $[1\bar{1}1]$ direction, the same direction along which the rows in figs. 5 and 6 are oriented. The intersection of the $(1\bar{2}1)$ plane and the (110) surface is in the $[\bar{1}13]$ direction, the same direction in which the rows in figs. 3 and 4 are aligned. The CS displacement is always of the type $\frac{1}{2}\langle 0\bar{1}1\rangle$, which

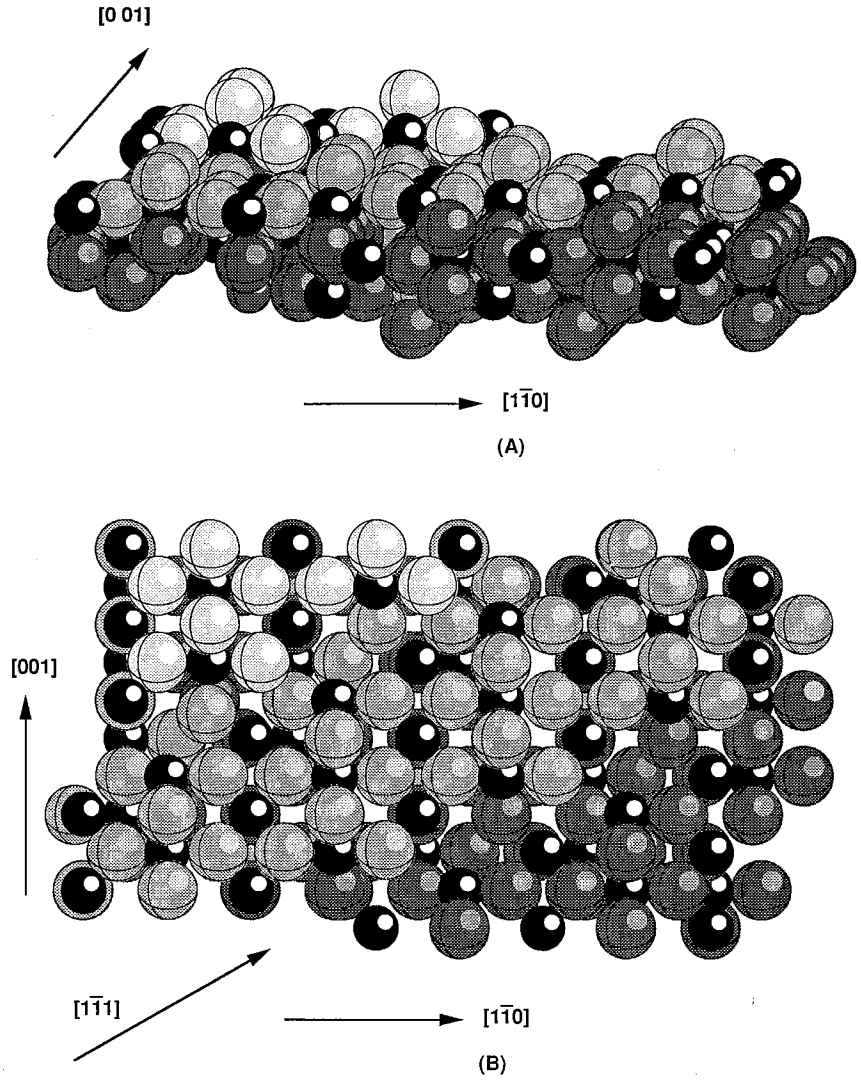

Fig. 8. Model of the sheared titania surface with local composition Ti_3O_5. Indicated directions refer to the rutile lattice vectors. (A) A glancing angle view of the surface showing the upward displacement of atoms that occurs at the CS plane/surface intersection. (B) View normal to the surface. In each case, oxygen atoms with darkest shading are on the lowest surface plane and the atoms with the lighter shading are on elevated surface planes.

means that adjacent sections of the crystal are vertically displaced 1.6 Å with respect to one another along the line normal to the (110) surface. This effectively creates a stepped surface. Surface slopes predicted by this model range from 3° to 10°, depending on the extent of reduction. While the measured image slopes are consistent with the surface slope predictions, they also fall within the uncertainty with which the surface slope is determined by the image slope.

Assuming this model to be true, the local stoichiometry can be determined simply by measuring the distance between adjacent CS plane/surface intersections. As the frequency of the planes increases, so does the metal-to-oxygen ratio. The spacing of the rows in fig. 5 (8–9 Å) suggests that every 6th anion (121) plane is a CS plane and that the local composition in this area is Ti_3O_5, while the spacing of the rows in fig. 4 (21 Å) suggests that CS occurs at every 8th anion $(1\bar{2}1)$ plane and that the local composition is Ti_4O_9. Although it is difficult to determine the precise spacing between the rows in the first structure type, the average spacing of about 33 Å suggests that the local composition is Ti_6O_{11}.

If this model is correct, it should also provide a mechanism to produce the contrast observed within the terraces formed by the CS plane/surface intersections. Consider, for example, the corrugations within the rows of the third structure type, which have a period of 3.2 Å. A model of this surface was constructed and is shown in fig. 8. The model was constructed simply by eliminating the O atoms along two (121) rutile planes, and changing the atomic positions of adjacent sections of the crystal by the shear displacement vector. The original surface was assumed to have the bridging oxygen atoms in place, but only surface oxygen ions that are two- or three-fold coordinated with Ti ions have been retained following the shear operations. The distance between the observed corrugations within the rows of the third structure type is nearly the same as the distance between Ti atoms along the edge of the shear planes. The periodicity of these Ti atoms, or more accurately the unoccupied electronic states associated with them, is a possible source of the observed contrast. A second undercoordinated Ti atom, which shares a face with a subsurface Ti octahedron, is located at the edge of the next row and in the same direction as the long axis of the elliptical surface unit observed in the topographic images. Such a group of atoms, incompletely resolved, could produce the observed images.

A similar model can be used to explain the patterns observed within the terraces of the second structure type. The separation of the links agrees with the distance between undercoordinated Ti atoms that would occur along the CS plane/surface intersection. The separation between the three units that make up each link also correlates with the distance between Ti atoms in that direction. The inequivalence in the size of the units might be related to the difference in coordination between the Ti atoms on the terrace and those on the edge created by the CS plane/surface intersection.

The *IV* curves from the bare surface demonstrate that, as expected, the Fermi level is pinned near the bottom of the conduction band edge. No significant current is measured in the negative bias region, since the nearest occupied electronic states should be about 3 eV below the conduction band edge. The similarity of the 10 sequential *IV* curves suggests that the data are not sensitive the the observed topographic corrugation. However, the potential to spectroscopically probe differences on the surface was demonstrated by measuring the tunneling spectrum of a surface protrusion. Although it is impossible to be certain as to the identity of this surface feature, we presume that it is associated with the carbon contamination detected by AES. The tunneling spectrum indicates that this surface feature is electronegative in character, since it creates occupied states in the bandgap.

Although the CS plane model successfully explains many aspects of the observations, two inconsistencies remain and are discussed below. The first is the difference between the observed real-space surface structural periodicities and the LEED patterns, which indicated a (1×1) pattern. We suggest that the cause of this inconsistency is rooted in the measurement techniques. The LEED pattern emphasizes average structural

periodicities, while local deviations from periodicity contribute only to the background. The STM, on the other hand, makes only local observations. It is possible that while a significant fraction of the surface had the (1×1) periodicity, the rest was made up of domains of the substoichiometric phases which, because of their small size and different orientations, contributed only to the background of the LEED pattern. The fact that no (1×1) surface regions were observed in the STM images might indicate that the measurement is, to some extent, self-selecting. The reduced conductivity in the stoichiometric (1×1) regions might have resulted in an unstable tunnel current which prevented the formation of high resolution images. A second inconsistency is that, according to accepted bulk thermodynamic data, the observed Magnéli phases should not have been produced by the heat treatments to which the crystal was subjected [21]. In fact, after STM analysis, the proposed phases could not be detected using X-ray diffraction. One possible explanation is that the CS phases nucleate heterogeneously at imperfections on the surface under the conditions of the experiment, but are kinetically limited from propagating through the bulk, a process which demands the migration of O vacancies and Ti interstitials over larger distances [22].

5. Conclusion

The goal of the work described in this paper was to clarify the structure of the TiO_{2-x}(110) surface using the real-space imaging capabilities of the STM. Our experiments have yielded interesting results that have been interpreted in terms of a model involving the nucleation of substoichiometric phases on the surface during heating in UHV. These observations provide new insight into the atomic level structure of this surface, and they demonstrate the structural diversity and complexity which can exist on metal oxide surfaces.

Acknowledgements

This work was supported at the University of Pennsylvania by the National Science Foundation under Grant DMR-8819885 and at Yale University by National Science Foundation Solid State Chemistry Grant DMR-8711423. We thank Zhaoming Zhang for assistance in preparing the sample surface.

References

[1] V.E. Henrich, Rep. Prog. Phys. 48 (1985) 1481.
[2] W. Göpel, Prog. Surf. Sci. 20 (1985) 9.
[3] G. Rocker and W. Göpel, Surf. Sci. 181 (1987) 530.
[4] V.E. Henrich, Prog. Surf. Sci. 9 (1979) 143.
[5] R.G. Egdell, S. Eriksen and W.R. Flavell, Solid State Commun. 60 (1986) 835.
[6] L.A. Bursill and B.G. Hyde, in: Prog. in Solid State Chemistry, Vol. 7, Eds. H. Reiss and J.O. McCaldin (Pergamon, New York, 1972) p. 177.
[7] J.B. Goodenough, in: Progress in Solid State Chemistry, Vol. 5, Ed. H. Reiss (Pergamon, New York, 1971) p. 145.
[8] S. Munnix and M. Schmeits, Phys. Rev. B 30 (1984) 2202.
[9] S.E. Gilbert and J.H. Kennedy, J. Electrochem. Soc. 135 (1988) 2385.
[10] S.E. Gilbert and J.H. Kennedy, Langmuir 5 (1989) 1412.
[11] K. Itaya and E. Tomita, Chem. Lett. (1989) 285.
[12] K. Sakamaki, S. Matsunaga, K Itoh, A. Fujishima and Y. Gohshi, Surf. Sci. 219 (1989) L531.
[13] K. Sakamaki, K. Itoh, A. Fujishima and Y. Gohshi, J. Vac. Sci. Technol. A 8 (1990) 614.
[14] S.E. Gilbert and J.H. Kennedy, Surf. Sci. Lett. 225 (1990) L1.
[15] R.F. Fan and A.J. Bard, J. Phys. Chem. 94 (1990) 3761.
[16] G.S. Rohrer, V.E. Henrich and D.A. Bonnell, Science 250 (1990) 1239.
[17] No ultraviolet photoelectron spectroscopy (UPS) data were taken on this surface, although the LEED patterns were similar to those on the TiO_2(110) surfaces that exhibit no bandgap defect surface states; see H.R. Sadeghi and V.E. Henrich, Appl. Surf. Sci. 19 (1984) 330.
[18] The STM head was manufactured by WA Technologies, Cambridge, England.
[19] J.K. Gimzewski and R. Moller, Phys. Rev. B 36 (1987) 1284.
[20] G.S. Rohrer and D.A. Bonnell, J. Am. Ceram. Soc. 73 (1990) 3026.
[21] Using estimated conditions of $T = 900$ K and $P_{O_2} = 1 \times 10^{-13}$ atm it is unlikely that the value of x in TiO_{2-x} exceeded 1×10^{-4} [6].
[22] J.S. Anderson, in: Intercalation Chemistry, Eds. M.S. Whittingham and A.J. Jacobson (Academic Press, New York, 1982) p. 503.